Crack Growth Properties of Sealing Glasses

J. Salem
NASA Glenn Research Center, Cleveland, OH, USA

R. Tandon
Sandia National Laboratories, Albuquerque, NM, USA

Keyword: glass, ceramics, strength, crack growth, fracture toughness, connectors

Abstract

The crack growth properties of several sealing glasses were measured using constant stress rate testing in 2% and 95% RH (relative humidity). Crack growth parameters measured in high humidity are systematically smaller (n and B) than those measured in low humidity, and velocities for dry environments are ~100x lower than for wet environments. The crack velocity is very sensitivity to small changes in RH at low RH. Confidence intervals on parameters that were estimated from propagation of errors were comparable to those from Monte Carlo simulation.

Introduction

Sealing glasses are used in components such as electrical feed through connectors. The glass seals and electrically insulates the connector, and thus fracture of the brittle seal is a concern. In applications such as the Space Shuttle Environmental Cut Off (ECO) system, the connector seals are subjected to differential pressures at cryogenic temperatures and seal failure can create leakage of dangerous liquids and/or gasses.

The crack growth properties of several sealing glasses were measured to compare glasses and to help perform life prediction and reliability of components such as feed through connectors. Strength based measurements, which are convenient, were used to generate the data. However, because the statistical scatter in parameters derived from strength data can be very large, the statistical significance of the estimates was checked by estimation of confidence intervals on the parameters via propagation of errors (POE) and Monte Carlo methods. The large scatter is a result of strength not being a material property for glasses, but a function of the fracture toughness and worst flaw size present from a variety of sources. Ideally, parameter estimation and design of brittle materials should be done on a fracture mechanics basis (e.g. NASGRO [1]) rather than a strength basis because strength is a function of the highly variable flaw size and relatively consistent fracture toughness.

Although fracture mechanics specimens with large cracks, such as the double-torsion specimen, can be used to measure crack growth with less scatter, the results are complicated by R-curve effects in coarse grain materials such as ZnSe [2] and diffusion rate effects when the crack size is large relative to that in real components. Strength based testing can be made more akin to fracture mechanics methods by placing a small precrack, such as an indentation, in specimens and thereby reduce scatter, yet test cracks

on the order of those encountered in applications. Comparison of sealing glass parameters from strength and fracture mechanics methods is left to future study.

In order to cover the range of environments to which components with sealing glasses are exposed, RH (relative humidity) of ~2% and 95% were considered. To expedite the work, constant stress rate testing of flexure specimens was used. The data was analyzed by linear regression of (1) the individual data points, (2) the median values, and (3) the average values.

Materials

The materials tested[1] were Corning 0120 sealing glass, Electro-Glass 2164, Schott 8330 borofloat glass, and Schott S-8070 SB glass-ceramic. In addition, the fracture toughness of several other glasses was measured for comparison: soda-lime silicate, S8061 sealing glass, and an antimony (Sb) doped glass. With the exception of the as-molded 2164 glass, the test specimens were prepared by diamond grinding in conformance with ASTM C1161 [3]. For the 2164 glass specimens for crack growth testing, the tensile surface was preserved in the as-molded condition.

Experimental Procedure

The elastic modulus of 2164 glass was determined at 20°C by impulse excitation of vibration in accordance with ASTM C 1259 [4]. The mean and standard deviation of seven specimens in the as-molded and ground conditions were 62.0 ± 1.2 and 63.8 ± 0.5 GPa respectively.

Fracture strength as a function of stress rate was measured at 20°C by using four point flexure of ASTM C1161 size B specimens [3] at rates ranging from 10^{-3} to 10^{3} MPa/s in relative humidity ranging from ~2% to 95%. Typically, six stress rates were applied with at least five specimens per rate. For the purposes of parameter analysis, the inert strength was determined by testing at low RH (<2%) with a stress rate greater than or equal to 1000 MPa/s. This results in failure in a fraction of a second.

Fracture toughness was measured by using chevron-notch flexure specimens [5] in laboratory ambient (~30% RH) air and dry nitrogen. Test specimen stability was monitored via a strain gage placed on the compressive face of the specimen [6].

Data Analysis

The power law formulation:

$$v = \frac{da}{dt} = AK_I^n = A^* \left[\frac{K_I}{K_{IC}}\right]^n \qquad (1)$$

was applied in the data analysis, where *v, a,* and *t* are crack velocity, crack size, and time, respectively. *A* and *n* are the material/environment dependent SCG (slow crack growth) parameters, and K_I and K_{IC} are, respectively, the Mode *I* stress intensity factor and the

[1] Certain commercial materials are identified in order to adequately specify the experimental procedure and results. Such identification does not imply any endorsement.

critical stress intensity factor or fracture toughness of the material under Mode *I* loading. For constant stress rate testing based on the power law formulation, the fracture strength, σ_f, is expressed as a function of stress rate as [7]

$$\sigma_f = \left[B(n+1)\sigma_i^{n-2}\dot{\sigma}\right]^{1/n+1} \tag{2}$$

where $\dot{\sigma}$ is the applied stress rate, σ_i is the inert strength, and B is a parameter associated with A, n, fracture toughness, crack geometry and loading configuration. The SCG parameter n can be determined from a plot of log σ_f as a function of log $\dot{\sigma}$ with Eq. 2 written as

$$\log \sigma_f = \frac{1}{n+1}\log \dot{\sigma} + \log D \tag{3}$$

where

$$\log D = \frac{1}{n+1}\log\left[B(n+1)\sigma_i^{n-2}\right] \tag{4}$$

Once the slope α and intercept β are estimated by linear regression of Eq. 3, the parameters n, D, B and A, and their standard deviation SD_n, etc., were estimated from [8]

$$n = \frac{1}{\alpha} - 1 \tag{5}$$

$$SD_n \approx \frac{SD_\alpha}{\alpha^2} \tag{6}$$

$$D = 10^\beta \tag{7}$$

$$SD_D \approx 2.3026\left(SD_\beta\right)\left(10^\beta\right) \tag{8}$$

$$B = \frac{\alpha\left(10^{\beta/\alpha}\right)}{\sigma_i^{\left(\frac{1}{\alpha}-3\right)}} \tag{9}$$

$$SD_{\ln B} \approx \frac{1}{\alpha}\sqrt{Q^2\frac{SD_\alpha^2}{\alpha^2} + (\ln 10)^2 SD_\beta^2 + (1-3\alpha)^2 SD_{\ln\sigma_i}^2 + 2Q\ln 10\frac{Cov(\alpha,\beta)}{\alpha}} \tag{10}$$

$$A^* = \frac{2K_{Ic}^2\sigma_i^{\left(\frac{1}{\alpha}-3\right)}}{10^{\beta/\alpha}(1-3\alpha)Y^2} = \frac{2K_{Ic}^2}{B(n-2)Y^2} \tag{11}$$

$$SD_{\ln A^*} \approx \frac{1}{\alpha}\sqrt{\begin{matrix}4\alpha^2\frac{SD_{K_{Ic}}^2}{K_{Ic}^2}+\left(Q-\frac{\alpha}{1-3\alpha}\right)^2\frac{SD_\alpha^2}{\alpha^2}+(\ln 10)^2 SD_\beta^2 \\ +(1-3\alpha)^2 SD_{\ln\sigma_i}^2+2\ln 10\left(Q-\frac{\alpha}{1-3\alpha}\right)\frac{Cov(\alpha,\beta)}{\alpha}\end{matrix}} \tag{12}$$

$$A=\frac{2K_{Ic}^{\left(3-\frac{1}{\alpha}\right)}\sigma_i^{\left(\frac{1}{\alpha}-3\right)}}{10^{\beta/\alpha}(1-3\alpha)Y^2}=\frac{2K_{Ic}^{2-n}}{B(n-2)Y^2} \tag{13}$$

$$SD_{\ln A} \approx \frac{1}{\alpha}\sqrt{\begin{matrix}(3\alpha-1)^2\frac{SD_{K_{Ic}}^2}{K_{Ic}^2}+\left(Q-\frac{\alpha}{1-3\alpha}-\ln K_{Ic}\right)^2\frac{SD_\alpha^2}{\alpha^2}+(\ln 10)^2 SD_\beta^2 \\ +(1-3\alpha)^2 SD_{\ln\sigma_i}^2+2\ln 10\left(Q-\frac{\alpha}{1-3\alpha}-\ln K_{Ic}\right)\frac{Cov(\alpha,\beta)}{\alpha}\end{matrix}} \tag{14}$$

where $$Q=\alpha-\beta\ln 10+\ln\sigma_i$$

and $$Cov(\alpha,\beta)=-SD_\alpha^2\left(\overline{\log\dot{\sigma}}\right) \tag{15}$$

where $\overline{\log\dot{\sigma}}$ is the mean of the log of the applied stressing rates, Y is the geometry correction factor for the stress intensity factor, and the standard deviation associated with the inert strength $(SD_{\ln\sigma i})$ is calculated in logarithmic space. Probability limits on the parameters B and A can be calculated from:

$$B_{\substack{Upper\\Lower}}=EXP\left[\ln B\pm t\left(SD_{\ln B}\right)\right] \quad \text{and} \quad A_{\substack{Upper\\Lower}}=EXP\left[\ln A\pm t\left(SD_{\ln A}\right)\right] \tag{16}$$

by using Student's t distribution for the DOF and probability level desired. If the DOF (degrees-of-freedom) is greater than ~40, then

$$B_{\substack{Upper\\Lower}}=EXP\left[\ln B\pm \ell\left(SD_{\ln B}\right)\right] \text{ and } A_{\substack{Upper\\Lower}}=EXP\left[\ln A\pm \ell\left(SD_{\ln A}\right)\right] \tag{17}$$

where ℓ is the number of standard deviations corresponding to the probability level desired. The DOF, ϕ, is given by

$$\begin{aligned}\frac{\left(SD_{\ln B}^2\right)^2}{\varphi_{\ln B}}=&\frac{1}{\varphi_{\ln\sigma_i}}\left[\frac{(1-3\alpha)^2}{\alpha^2}SD_{\ln\sigma_i}^2\right]^2+\\ &\frac{1}{\varphi_{\alpha\beta}}\left[Q^2\frac{SD_\alpha^2}{\alpha^4}+(\ln 10)^2\frac{SD_\beta^2}{\alpha^2}+2Q\ln 10\frac{Cov(\alpha,\beta)}{\alpha^3}\right]^2\end{aligned} \tag{18}$$

and

$$\frac{\left(SD_{\ln A}^2\right)^2}{\varphi_{\ln A}} = \frac{1}{\varphi_{\ln K_{Ic}}}\left(4SD_{\ln K_{Ic}}^2\right)^2 + \frac{1}{\varphi_{\ln \sigma_i}}\left[\frac{(1-3\alpha)^2}{\alpha^2} SD_{\ln \sigma_i}^2\right]^2 + \frac{1}{\varphi_{\alpha\beta}}\left[\left(Q - \frac{\alpha}{1-3\alpha}\right)^2 \frac{SD_\alpha^2}{\alpha^4} + (\ln 10)^2 \frac{SD_\beta^2}{\alpha^2} + 2\ln 10\left(Q - \frac{\alpha}{1-3\alpha}\right)\frac{Cov(\alpha,\beta)}{\alpha^3}\right]^2 \quad (19)$$

where φ_{σ_i} is the DOF in inert strength (number of inert strength tests minus one) and $\phi_{\alpha\beta}$ is the DOF in regression (number of constant stress rate tests minus two).

Three approaches were used to estimate the slope and intercept of eq. 3: linear regression of (1) the individual data points; (2) the median values; and (3) the average values. In addition to the approaches described, the fits were performed over several stress rate ranges to determine the sensitivity to data range.

Results

Fracture Toughness

Examples of load-backface strain curves for laboratory air and dry N_2 are shown in Figure 1 for the Electro-Glass 2164. Stable fracture was exhibited in both environments; however, less stability was exhibited in dry N_2. Fracture toughness in dry N_2 ranged from 0.72 to 0.80 MPa√m for the glasses, as summarized in Table 1. Testing in air reduced the measured fracture toughness by ~10%. For the purposes of crack growth parameter estimation, the fracture toughness the 0120, 8070 and 8330 materials, which were not measured, were assumed to be 0.75 ± 0.04 MPa√m.

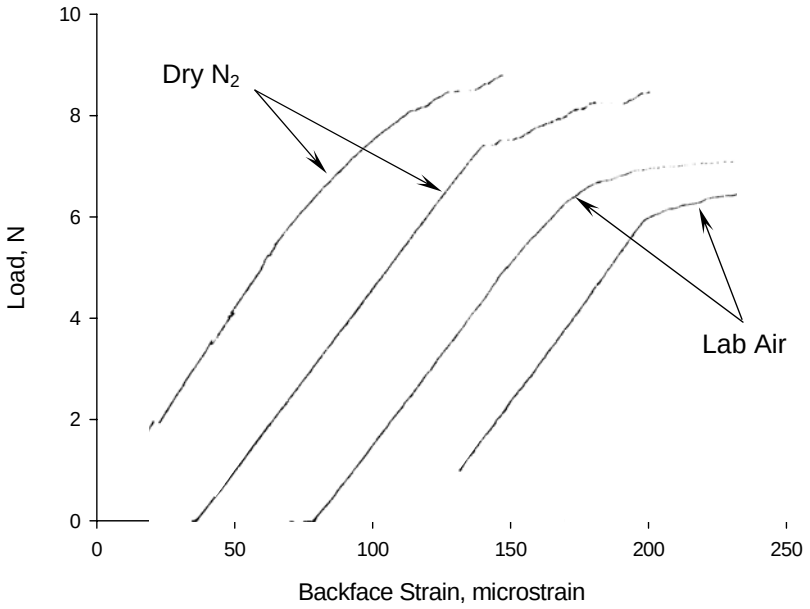

Figure 1 Load as a function of backface strain for Electro-glass 2164 chevron-notched flexure specimens in dry nitrogen and laboratory air.

Table 1 Fracture toughness (MPa√m) of several glasses

Material	Environment	
	Air (%RH/^{o}F)	**Dry N_2**
S8061	0.64 ± 0.01 (23/73)	0.72 ± 0.02
2164	0.61 ± 0.05 (32/73)	0.74 ± 0.03
Soda lime silicate	0.75 ± 0.04 (35/73)	0.80 ± 0.01
Sb-doped	0.72 ± 0.002 (23/73)	0.76 ± 0.01

Inert and Time-dependant Strength

The strength as a function of stress rate is plotted in Figures 2–5. The large degree of scatter, particularly at low RH, is indicative of the difficulty in characterizing and designing glasses and dense optical materials with the inherent flaw population and strength measurements: random and spurious damage make the distribution ever changing and difficult to characterize, regardless of Weibull statistics. In this testing, the effect of scatter on slow crack growth was mitigated partially by the large range of stress rates used (>4 orders of magnitude). All the materials, except the 8070 SB glass-ceramic, exhibit a strength increase from ~50 MPa in 95% RH to ~150 MPa in 2% RH as the stress rate is increased from 0.001 MPa/s to 1000 MPa/s, implying a similar combination of flaw size distribution and fracture toughness. As the fracture toughness values are likely similar (Table I), the implication is a similar flaw size distribution.

The slow crack growth parameters as estimated from equations (5) to (17) are summarized in Table 2.

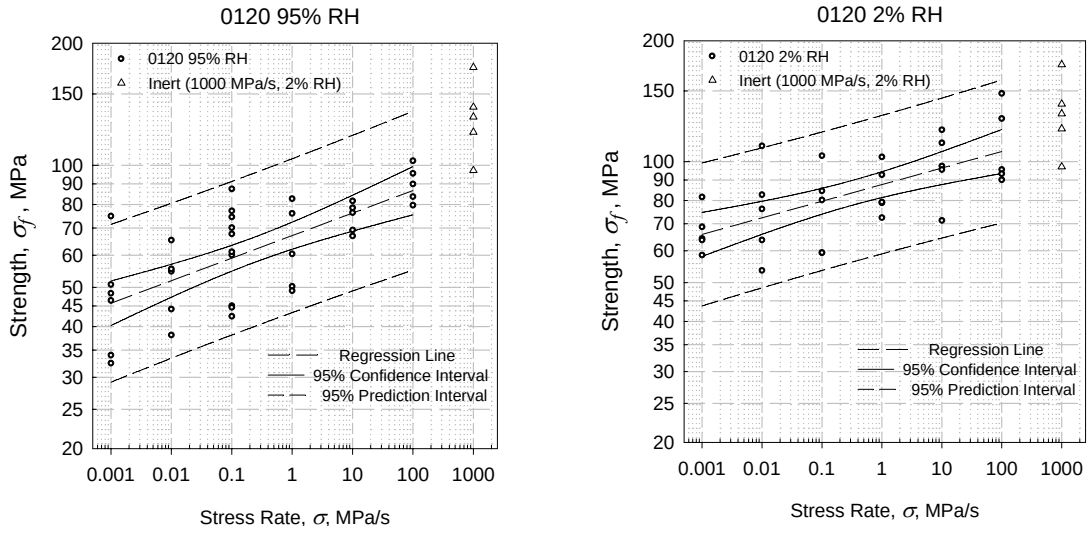

Figure 2 Strength of 0120 glass in 2% and 95% relative humidity.

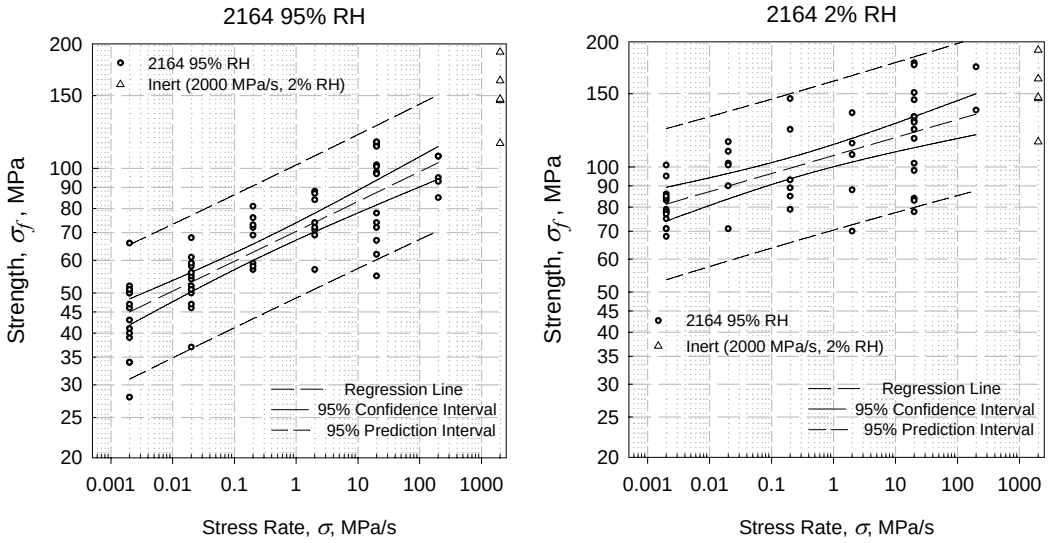

Figure 3 Strength of 2164 in 2% and 95% relative humidity.

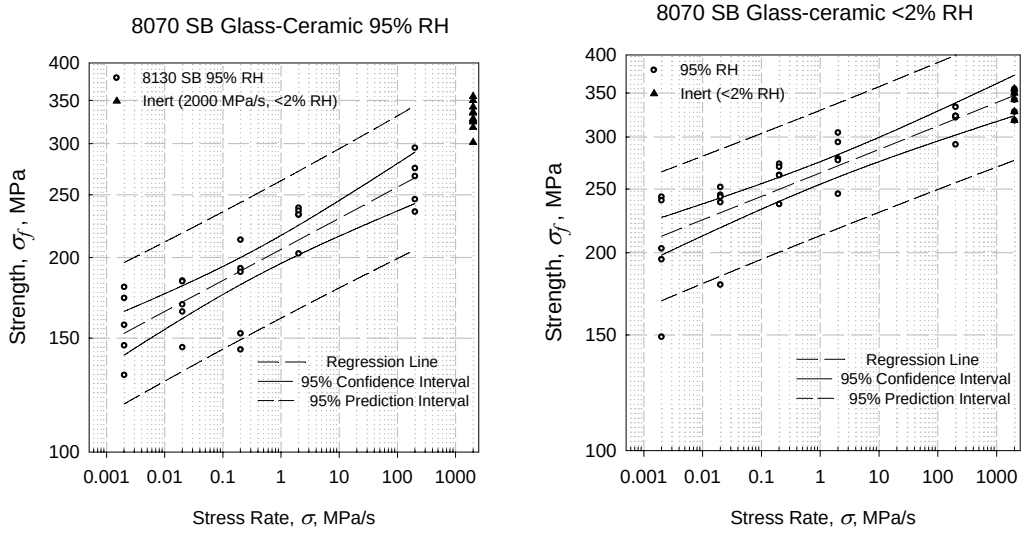

Figure 4 Strength of 8070 SB glass-ceramic in <2% and 95% relative humidity.

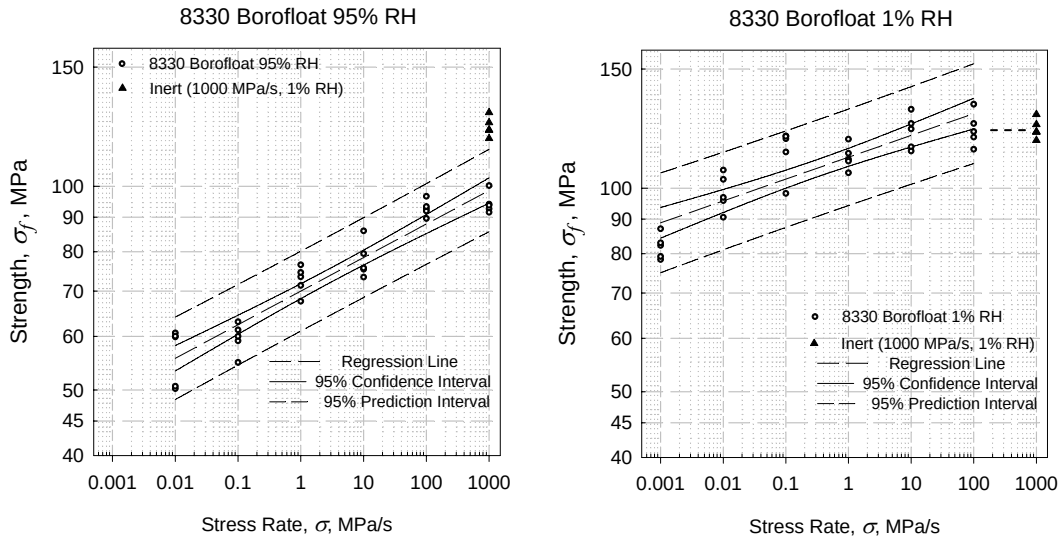

Figure 5 Strength of 8330 borofloat in 1% and 95% relative humidity.

Table 2 Summary of slow crack growth (SCG) parameters for glasses

Regression of Individual Points	***n***	***B*** $MPa^2 \cdot s$	$B_{-95\%}$	***A*** m/s $(MPa\sqrt{m})^{-n}$	$A_{+95\%r}$ m/s $(MPa\sqrt{m})^{-n}$	**# of SCG Tests**
0120, 95%	17.0 ± 3.1	0.6	1.8×10^{-4}	$4.4 \times 10^{+0}$	$3.9 \times 10^{+4}$	36
0120, 2%	23.2 ± 5.3	4.3	1.0×10^{-4}	$2.6 \times 10^{+0}$	$5.6 \times 10^{+5}$	30
2164, 95% RH	12.9 ± 1.1	6	.06	2.3×10^{-1}	$3.4 \times 10^{+1}$	65
2164, <2% RH	22.1 ± 3.9	39	.01	3.0×10^{-1}	$4.4 \times 10^{+3}$	48
8070 SB, 95% RH	19.8 ± 2.6	60	1.6	8.2×10^{-2}	$1.3 \times 10^{+1}$	25
8070 SB, <2% RH	25.0 ± 3.9	3,079	93	5.5×10^{-3}	$1.5 \times 10^{+0}$	25
8330, 95% RH	17.1 ± 1.3	5	0.7	5.6×10^{-1}	$1.0 \times 10^{+1}$	25
8330, <3% RH	24.5 ± 3.9	19	0.4	8.0×10^{-1}	$3.1 \times 10^{+2}$	30
8330, <1% RH	30.0 ± 3.6	2,855	266	2.1×10^{-2}	$2.3 \times 10^{+0}$	30
Sb-doped, Distilled Water	12.2 ± 0.4	12	1	1.1×10^{-1}	$1.3 \times 10^{+0}$	115
Sb-doped, 65%RH	13.1 ± 0.4	92	9	1.7×10^{-2}	2.4×10^{-1}	115
Soda-lime silicate, Distilled Water	20.0 ± 2.0	18	423	9.0×10^{-2}	$5.7 \times 10^{+0}$	30

Table 3 Comparison of fitting ranges and methods for the 8330 borofloat glass tested in 95% RH.

Fit Method	*n*	*B* $MPa^2 \cdot s$	*A* $m/s\ (MPa\sqrt{m})^{-n}$	*# Observations*
All Data (high rate included)				
Individual points	19.2 ± 1.3	1	3.7×10^{0}	30
Median values	21.6 ± 3.0	0.4	2.1×10^{1}	6
Average values	19.3 ± 2.0	1	3.9×10^{0}	6
< 1000 MPa/s (avoid inert region)				
Individual points	17.1 ± 1.3	5	5.6×10^{-1}	25
Median values	19.9 ± 3.6	1	4.5×10^{0}	5
Average values	17.2 ± 1.8	5	5.9×10^{-1}	5

Table 4 Comparison of fitting ranges and methods for the 8330 borofloat glass tested in 1% RH.

Fit Method	*n*	*B* $MPa^2 \cdot s$	*A* $m/s\ (MPa\sqrt{m})^{-n}$	*# Observations*
All Data (high rate included)				
Individual points	36.8 ± 4.4	608	5.5×10^{-1}	35
Median values	38.2 ± 11.2	541	9.0×10^{-1}	7
Average values	36.8 ± 8.8	632	5.4×10^{-1}	7
< 1000 MPa/s (avoid inert region)				
Individual points	30.0 ± 3.6	2855	2.1×10^{-2}	30
Median values	30.4 ± 8.7	3032	2.2×10^{-2}	6
Average values	30.0 ± 7.0	2984	2.0×10^{-2}	6

Table 5 Comparison of propagation-of-errors equations to Monte Carlo estimates

Material and Humidity	*B* $MPa^2 \cdot s$	$B_{-95\%}$ $MPa^2 \cdot s$	*A* $m/s\ (MPa\sqrt{m})^{-n}$	$A_{+95\%}$ $m/s\ (MPa\sqrt{m})^{-n}$
2164, 95% RH	5.7	0.06	0.230	34.1
Monte Carlo	6.1	0.11	0.217	20.2
2164, <2% RH	39	0.009	0.298	4,361
Monte Carlo	41	0.011	0.263	12,891

Discussion

Effects of Humidity

Table 2 demonstrates that lower test humidity results in higher estimates of *n* and *B*, regardless of the type of glass tested, implying that controlling or eliminating moisture via coatings, etc. will improve component life. The variances are also somewhat larger for dry conditions because the shallower slope is more difficult to characterize for the same x-axis range. The parameters are also very sensitive to small changes in humidity at low humidity: the value of *B* changes by a factor of ~100 for a change of 3% to 1% whereas a change from 95% to 3% only results in a factor of ~10 change.

Effect of Fit Method and Range

The effects of fit range and method on the estimated parameters can be seen in Tables 3 and 4: the fitting methods produce similar results for data set; and the inclusion of the high stress rate data (1000 MPa/s) substantially alters the results at low humidity by increasing *n*. The lack of an effect of fit method implies either few outliers or sufficient data to mitigate the influence of outliers. The effect of fit range can be mitigated by using crack growth data only from lower stress rates (< ~200 MPa/s) [9], and independently measuring inert strength with ~0%RH.

Confidence Intervals

The 95% confidence intervals on *B* for the sealing glasses in Table 2 differ from the estimates by 1 to 3 orders of magnitude, even for data sets with 60 observations. The relatively large confidence intervals on some of the data sets imply that the use of inherent or natural flaws requires very large data sets. In another study, the use of 115 tests to characterize the Sb-doped glass in Table 1 resulted in standard deviations on *n* of less than ¼ of those for the sealing glasses, and a 95% confident interval on *A* and *B* within one order of magnitude of the estimate, as shown in Table 2. Improvements can also be made by maximizing the range of rates used, and by performing most of tests at the highest and lowest rates. Monte Carlo estimates compared well with estimates from equations (5) to (17), as shown on Table 5.

Crack Velocity

The crack velocity as a function of stress intensity based on the estimated parameters in Table 2 is shown in Figures 6 and 7. The 8070 glass exhibited the least crack velocity whereas the 0120 and 2164 glasses exhibited the greatest velocities at any stress intensity. It should be noted that the fracture toughness of some of the glasses was not measured and the results could shift if the fracture toughness is significantly different than the assumed value of 0.75 MPa$\sqrt{m}$. Application of common time-to-failure equations [7] indicate the sustainable stress for the 8070 is doubled if the humidity is changed from 95% to 2%. As compared to soda-lime silicate float glass, the sealing glasses exhibit greater susceptibility to slow crack growth, as shown in Figure 6.

Conclusions

SCG parameters measured using constant stress rate testing in high humidity are systematically smaller (*n* and *B*) than those measured in low humidity. Velocities for dry environments are ~100x lower than for wet environments: keeping components dry should extend the life! The use of high stress-rate data increased estimates *n* at low RH, and thus should be used with caution. 8070 glass-ceramic exhibits the lowest crack velocities of the sealing glasses tested, and reducing RH from 95% to 2% nearly doubles the sustainable stress. The crack velocity is very sensitive to small changes in RH at low RH: for the 8330 glass, a ~100x change in velocity resulted for changes of RH from 1% to 3% and 3% to 95%. Monte Carlo simulations and propagation of errors solutions gave

similar estimates of parameter variance. Future work should include measurement of the fracture toughness of all the materials in order to more accurately estimate A, and measurement of the parameters with macro-crack test specimens for comparison.

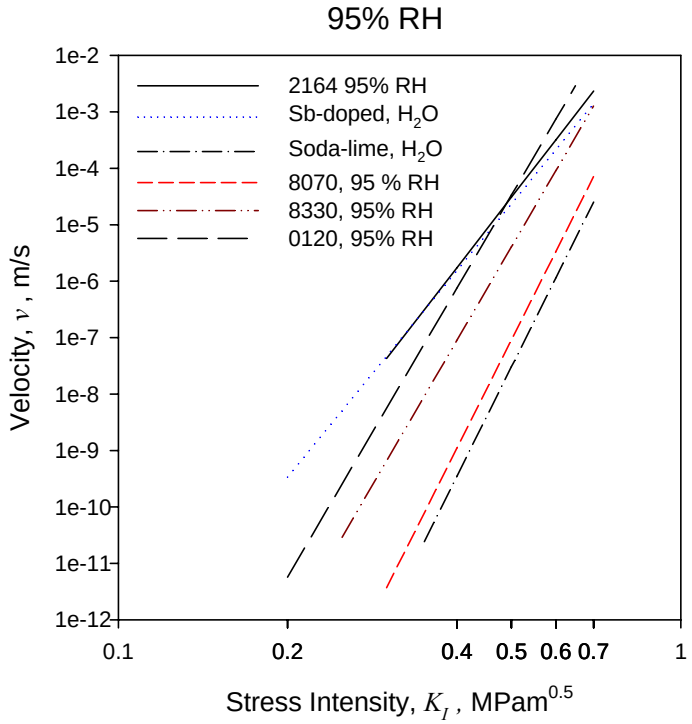

Figure 6 Crack velocity for 95% relative humidity based on the parameters in Table 2.

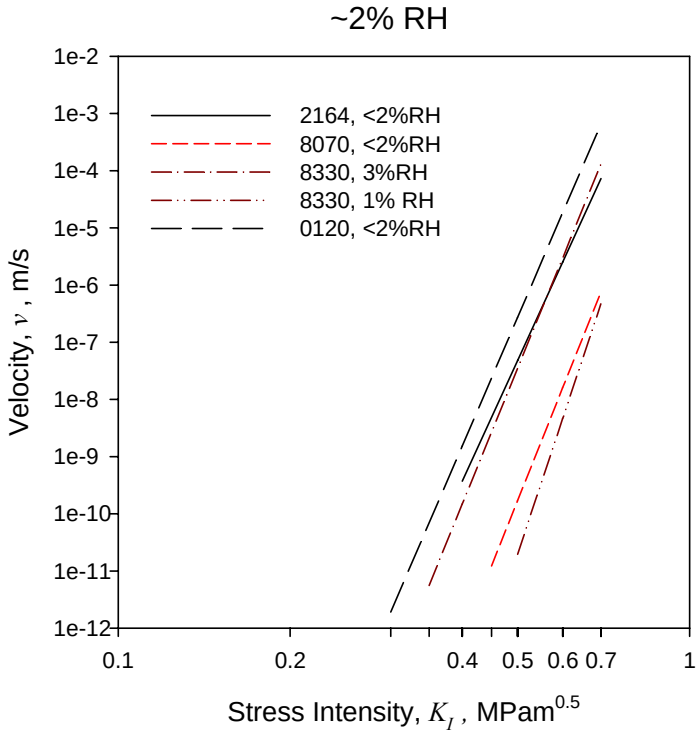

Figure 7 Crack velocity for 1 to 3% relative humidity based on the parameters in Table 2.

Acknowledgements

The authors thank J. Jill Glass for many useful discussions, and Frank Kody and Sara Caruso for running the soda-lime silicate SCG tests.

References

[1] NASGRO Fracture Mechanics and Fatigue Crack Growth Analysis Software, version 5.1, Southwest Research Institute, San Antonio, Texas.

[2] J.A. Salem “Mechanical Characterization of ZnSe Windows for use with the Flow Enclosure Accommodating Novel Investigations in Combustion of Solids (FEANICS) Module,” NASA TM 214100, 2006.

[3] ASTM C 1161, "Standard Test Method for Flexural Strength of Advanced Ceramics at Ambient Temperature," in *Annual Book of Standards*, Vol. 15.01, American Society for Testing and Materials, West Conshohocken, PA, 2004.

[4] ASTM C 1259, “Standard Test Method for Dynamic Young’s Modulus, Shear Modulus, and Poisson’s Ratio for Advanced Ceramics by Impulse Excitation of Vibration," in *Annual Book of Standards*, Vol. 15.01, American Society for Testing and Materials, West Conshohocken, PA, 2004.

[5] ASTM C 1421-99 “Standard Test Method for the Determination of Fracture Toughness of Advanced Ceramics at Ambient Temperatures,” in Annual Book of ASTM Standards, V. 15.01, American Society for Testing and Materials, West Conshohocken, Pennsylvania (2000).

[6] J.A. Salem and L. J. Ghosn, “Back-Face Strain as a Method For Monitoring Stable Crack Extension In Ceramics,” *Ceramic Engineering and Science Proceedings*, Vol. 19, No. 3, pp. 587-594, (1998).

[7] J.E. Ritter, "Engineering Design and Fatigue Failure of Brittle Materials," in *Fracture Mechanics of Ceramics*, Vol. 4, R. C. Bradt, D. P. H. Hasselman, and F. F. Lange, Eds., Plenum Publishing Co., NY, 1978, pp. 661-686.

[8] J.A. Salem and A.S. Weaver, “Estimation and Simulation of Slow Crack Growth Parameters from Constant Stress Rate Data,” pp. 579-596 in Fracture Mechanics of Ceramics: Active Materials, Nanoscale Materials, Composites, Glass, and Fundamentals, R.C. Bradt, D. Munz, M. Sakai and K. White, eds., Springer, (2005).

[9] J.A. Salem and M.G. Jenkins, “The Effect of Stress Rate on Slow Crack Growth Parameters,” pp. 213-227 in Fracture Resistance Testing of Monolithic and Composite Brittle Materials, ASTM STP 1409, J.A. Salem, G.D. Quinn and M.G. Jenkins, Eds., American Society for Testing and Materials, West Conshohocken, Pennsylvania (January, 2002).